Stratum corneum model membranes : molecular organization in relation to skin barrier function

Groen, D.

Chapter 3

Is an orthorhombic lateral packing and a proper lamellar organization important for the skin barrier function?

Daniël Groen, Dana S. Poole, Gert S. Gooris, Joke A. Bouwstra

Biochim Biophys Acta, vol. 1808, issue 6, pp. 1529-1537.

Abstract

The lipid organization in the stratum corneum (SC), plays an important role in the barrier function of the skin. SC lipids form two lamellar phases with a predominantly orthorhombic packing. In previous publications a lipid model was presented, referred to as the stratum corneum substitute (SCS), that closely mimics the SC lipid organization and barrier function. Therefore, the SCS serves as a unique tool to relate lipid organization with barrier function. In the present study we examined the effect of the orthorhombic to hexagonal phase transition on the barrier function of human SC and SCS. In addition, the SCS was modified by changing the free fatty acid composition, resulting in a hexagonal packing and perturbed lamellar organization. By measuring the permeability to benzoic acid as function of temperature, Arrhenius plots were constructed from which activation energies were calculated. The results suggest that the change from orthorhombic to hexagonal packing in human SC and SCS, does not have an effect on the permeability. However, the modified SCS revealed an increased permeability to benzoic acid, which we related to its perturbed lamellar organization. Thus, a proper lamellar organization is more crucial for a competent barrier function than the presence of an orthorhombic lateral packing.

1. Introduction

The uppermost layer of the human skin, the stratum corneum (SC), consists of flattened protein-rich dead cells (corneocytes) surrounded by intercellular lipids. The intercellular lipid domains in the SC form the only continuous pathway through the SC and are suggested to act as the main barrier for diffusion of substances through the SC (3). The main lipid classes in the SC are ceramides (CER), cholesterol (CHOL) and free fatty acids (FFA) (4-8). The lipids are arranged in two coexisting lamellar phases; a long periodicity phase (LPP) with a repeat distance of around 13 nm and a short periodicity phase (SPP) with a repeat distance of around 6 nm (9, 10). Furthermore, at the skin temperature of around 30-32°C in human SC the orthorhombic lateral packing is dominantly present, although a subpopulation of lipids also forms a hexagonal lateral packing. When increasing the temperature of SC, a transition is noticed from an orthorhombic to a hexagonal lateral packing between 30 and 40ºC. Both the lateral and lamellar lipid organization are considered to play an important role in the barrier function of the skin (11-13). A detailed analysis of the lipid composition revealed that the FFA have a wide chain length distribution, in which the chain lengths of 22 and 24 carbon atoms are most abundantly present (14). In addition, there are eleven subclasses of CER identified in human SC (4, 7, 8).

As the lipids play a crucial role in the barrier function, a large number of studies have been performed to understand the complex lipid phase behaviour underlying the skin barrier function. These studies, performed using isolated as well as synthetic CER mixtures, have markedly contributed to our present knowledge on the SC lipid organization and the role the lipid subclasses play in the lipid phase behaviour (12, 15-22). However, in these studies no information was obtained about the relation between lipid organization and skin barrier function. In order to study this, we developed a SC lipid model consisting of a porous substrate covered by a lipid film prepared from synthetic CER, CHOL and FFA. This lipid membrane mimics

the lipid organization and lipid orientation in SC closely and is referred to as the stratum corneum substitute (SCS) (23-25). As the lipid composition can easily be modified, this lipid membrane allows us to study the relationship between lipid composition, molecular organization and barrier function in just one model. In a previous study using the SCS, it was observed that the LPP plays an important role in the skin barrier function (23). However, only little information is available on the role the orthorhombic lateral packing plays in forming a proper skin barrier function. One of the key parameters to monitor the skin barrier function is the trans epidermal water loss (TEWL). In a very recent study the TEWL has been related to the degree of orthorhombic lateral packing present in SC in vivo in humans (26).

In the present study we examine whether the formation of the very dense orthorhombic packing and the formation of the characteristic lamellar phases observed in SC are crucial for the lipid barrier function in SC. As model compound we use benzoic acid (BA), a medium lipophilic low MW molecule. To examine the lipid organization in the SCS models, Fourier transform infrared spectrometry (FTIR) and small-angle x-ray diffraction (SAXD) are used. To determine the importance of the orthorhombic lateral packing for the SC lipid barrier, diffusion studies are performed during a step-wise increase in temperature from 15 to 45°C, sampling the temperature of the orthorhombic-hexagonal phase transition. To determine whether a simultaneous change in lateral packing and in the lamellar phases has a profound effect on the SC lipid barrier, a SCS with short free fatty acids is prepared, referred to as the short FFA SCS. This composition was selected as short chain FFAs are encountered in SC of human skin equivalents (27).

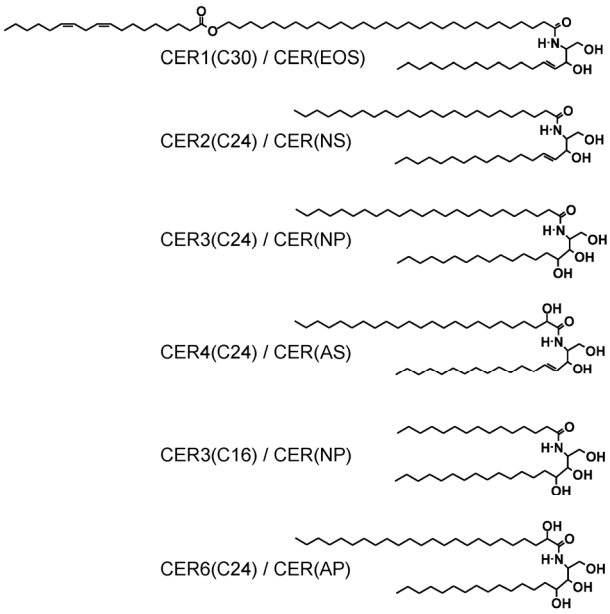

Figure 1: Molecular structure of the synthetic CER used in the SCS. The nomenclature is according to Motta et al (1).

2. Materials and Methods

2.1 Materials

In these studies we used 5 CER subclasses, see figure 1. The CER subclasses consist of either a sphingosine (S) or phytosphingosine (P) base, whereas the acyl chain is a nonhydroxy (N), α-hydroxy (A) or ω-hydroxy chain (1). The acyl chain length is either 16 carbons (C16), 24 carbons (C24) or 30 carbons (C30). The corresponding nonhydroxy and α-hydroxy CER are denoted as CER NS (C24), CER NS (C16), CER NP (C24) and CER AP (C24). In an additional CER subclass a linoleic acid is ester linked to the ω-hydroxy group (indicated by EO) with a sphingosine base. This CER is denoted as CER EOS (C30). These ceramides were generously provided by Cosmoferm B.V. (Delft, The Netherlands). Myristic acid (C14:0), palmitic acid (C16:0), stearic acid (C18:0), arachidic acid (C20:0), behenic acid (C22:0),

tricosanoic acid (C23:0), lignoceric acid (C24:0), cerotic acid (C26:0) and cholesterol were purchased from Sigma-Aldrich Chemie GmbH (Schnelldorf, Germany). The deuterated FFA with chain length of C16:0 and C22:0 were obtained from Larodan (Malmö, Sweden) and C14:0, C18:0 and C20:0 were purchased from Cambridge Isotope laboratories (Andover MA, USA). Benzoic acid, trypsin (type III, from bovine pancreas), and trypsin inhibitor (type II-S from soybean) were obtained from Sigma-Aldrich (Zwijndrecht, The Netherlands). Dialysis membrane disks (cutoff value of 5000 Da) were obtained from Diachema (Munich, Germany). Nuclepore polycarbonate filter disks (pore size 50 nm) were purchased from Whatman (Kent, UK). All organic solvents are of analytical grade and manufactured by Labscan Ltd. (Dublin, Ireland). All other chemicals are of analytical grade and the water is of Millipore quality.

2.2 Isolation of SC from human skin

SC was isolated from abdominal or mammary skin, which was obtained from the hospital within 24 h after cosmetic surgery. After removal of the subcutaneous fat tissue, the skin was dermatomed to a thickness of approximately 250 µm using a Padgett Electro Dermatome Model B (Kansas City KS, USA). The SC was separated from the epidermis by trypsin digestion [0.1% in phosphate-buffered saline (PBS), pH 7.4], after overnight incubation at 4°C and subsequently at 37°C for 1 h. The SC was then placed in a 0.1% solution of trypsin inhibitor and washed twice with Millipore water. Until use, the SC was stored in a silica-containing box under gaseous argon in the dark to prevent oxidation of the intercellular SC lipids. Before FTIR measurements, the SC was rehydrated for 24h at 100% relative humidity.

2.3 Preparation of the lipid mixtures

For the preparation of the SCS, synthetic CER, CHOL and FFA were used in equimolar ratio. For the SCS, the following synthCER composition was selected (see also figure 1): CER EOS (C30), CER NS (C24), CER NP

(C24), CER AS (C24), CER NP (C16) and CER AP (C24) in a 15:51:16:4:9:5 molar ratio, similar as observed in pig SC (16). For the free fatty acid mixture (FFA), the following composition was selected: C16:0, C18:0, C20:0, C22:0, C23:0, C24:0 and C26:0 at a molar ratio of 1.8:4.0:7.7:42.6:5.2:34.7:4.1 respectively. This chain length distribution is based on the reported FFA composition in SC (14). For the model with shorter FFA chain length, a FFA mixture with the following composition was used; C14:0, C16:0, C18:0, C20:0 and C22:0 in molar ratios of 8.9:43.5:38.6:4.3:4.7. The same composition and molar ratios were used for the deuterated short chain FFA mixture used in FTIR studies. For each SCS model the appropriate amount of individual lipids was dissolved in hexane:ethanol (2:1 v/v) at a lipid concentration of 4.5 mg/ml.

Preparation of the lipid mixture for FTIR was the same as above, but instead 1.5 mg of lipids was dissolved in chloroform:methanol (2:1, v/v).

2.4 Spraying of the lipid mixtures onto a porous substrate for use in permeation studies, small angle X-ray diffraction measurements and electron microscopic studies

A Camag Linomat IV (Muttenz, Switzerland) was extended with a y-axis arm. The linomat device makes use of a Hamilton syringe (100 µl) and mechanics to spray a confined (programmable) volume of sample solution (lipids in hexane:ethanol at 4.5 mg/ml concentration) from a distance of 1 mm onto the porous filter substrate. With the y-axis arm, the linomat is capable of spraying lipids in a rectangular shape by a continuous zigzag movement. The spraying flow rate is 5.0 µl/min under a stream of nitrogen gas at a movement speed of 1 cm/s. The area of spraying is 8×8 mm. The amount of lipid solution used is 200 µl per SCS. After spraying, the lipid films were equilibrated for 10 minutes at elevated temperature. The SCS and short FFA SCS were equilibrated at 80ºC and 60ºC respectively. After equilibration, the membranes were cooled down to room temperature in approximately 30 minutes.

2.5 Spraying of the lipid mixtures onto a AgBr window for use in fourier transform infrared studies

Sample preparation for FTIR was the same as above, but instead 1.5 mg of lipids was sprayed by the Linomat from chloroform:methanol (2:1, v/v) in an area of 1 cm^2 on an AgBr window. The sample was equilibrated for 10 min and slowly cooled down to room temperature. The SCS and short FFA SCS were equilibrated at 80ºC and 60ºC respectively. Subsequently, the lipid layer was covered with 25 µl of deuterated acetate buffer pH 5 (50 mM). After buffer application, the sample was kept at 37°C for 24h to obtain a full hydration. Finally, to homogenize the sample, five freeze-thawing cycles of 3h each were carried out between -20°C and RT (28).

2.6 Permeability studies

In vitro permeation studies were performed using Permegear inline diffusion cells (Bethlehem PA, USA) with a diffusion area of 0.28 cm^2. The SC was supported by a dialysis membrane (5000 Da, apical side facing the donor chamber). The SC and SCS were mounted in the diffusion cells and were hydrated for 1 h in phosphate-buffered saline (PBS: NaCl, Na_2HPO_4, KH_2PO_4 and KCL in MQ water with a concentration of 8.13, 1.14, 0.20 and 0.19 g/l respectively) at pH 7.4 prior to the experiment. The donor compartment was filled with 1.4 ml of BA (MW 122 g/mol) solution in PBS (pH 7.4) at a 2.0 mg/ml concentration. BA has a $\log K_{o/w}$ value of 1.7. The acceptor phase consisted of PBS (pH 7.4), which was perfused at a flow rate of about 2 ml/h and was stirred with a magnetic stirrer. The volume per collected fraction was determined by weighing. Each experiment was performed under occlusive conditions, by closing the opening of the donor compartment with adhesive tape. The temperature of the SC or SCS during permeation was controlled by a thermo-stated water bath. To determine the activation energy for permeation, at predetermined time intervals the temperature of the SCS or SC was increased in steps of 3°C within a time interval of 10 min. Fractions were collected at a 1 h interval. Steady state

fluxes (J_{SS}) were calculated from the horizontal part of the flux profile. For the data analysis, the following Arrhenius-type equations were used (29):

$$D = \frac{D_0}{\exp(E_D/RT)} \qquad \text{or} \qquad \ln(D) = \ln(D_0) - \frac{E_D}{RT} \quad (1)$$

Where R is the gas constant, D is the diffusivity of the permeating compound and D_0 denotes the hypothetical diffusivity at infinite temperature. During steady state conditions, the flux equals to:

$$J_{SS} = \frac{C \cdot K \cdot D}{L} \qquad (2)$$

In which C, and K are respectively the donor concentration (under sink conditions) and partition coefficient of the permeating compound, while L is the penetration pathlength through SC or SCS. Since D is strongly related to temperature (see equation 1) and K and L are only moderately affected by the temperature, we can rewrite equation 1 by using equation 2 to obtain:

$$R\ln(J_{SS}) = R\ln(J_{SS_0}) - E_P(1/T) \quad (3)$$

Following equation 3, the natural logarithm of the obtained steady state fluxes (multiplied by the gas constant) was plotted as function of the inverse absolute temperature. Subsequently, the activation energy for permeation (E_p) was calculated directly from the slope of a linear fit through the data.

2.7 Fourier Transform Infrared spectral measurements

All spectra were acquired on a BIORAD FTS4000 FTIR spectrometer (Cambridge MA, USA) equipped with a broad-band mercury cadmium telluride detector, cooled by liquid nitrogen. The sample cell was closed by two AgBr windows. The sample was under continuous dry air purge starting 1 hour before the data acquisition. The spectra were collected in transmission mode, as a co-addition of 256 scans at 1 cm^{-1} resolution during 4 minutes. In order to detect phase transitions, the sample

temperature was increased at a heating rate of 0.25°C/min resulting in a 1°C temperature rise per recorded spectrum. The spectra were collected between 0°C and 90°C and deconvoluted using a half-width of 5 cm^{-1} and an enhancement factor of 2.0. The software used was Win-IR pro 3.0 from Biorad.

2.8 Small-angle x-ray diffraction measurements

Small-angle x-ray diffraction (SAXD) was used to obtain information about the lamellar organization (i.e., the repeat distance of a lamellar phase). The scattering intensity I (in arbitrary units) was measured as function of the scattering vector q (in reciprocal nm). The latter is defined as $q=(4\pi\sin\theta)/\lambda$, in which θ is the scattering angle and λ is the wavelength. From the positions of a series of equidistant peaks (q_n), the periodicity, or d-spacing, of a lamellar phase was calculated using the equation $q_n=2n\pi/d$, with n being the order number of the diffraction peak. One-dimensional intensity profiles were obtained by transformation of the 2D SAXD detector pattern from Cartesian (x,y) to polar (ρ,θ) coordinates and subsequently integrating over θ. All measurements were performed at the European Synchrotron Radiation Facility (ESRF, Grenoble) using station BM26B. The x-ray wavelength and the sample-to-detector distance were 0.113 nm and 0.419 m respectively. Diffraction data were collected on a Frelon 2000 CCD detector with 2048×2048 pixels of 14 μm spatial resolution at 5x magnification. The spatial calibration of this detector was performed using silver behenate (d=5.838 nm) and the two strongest reflections of high density polyethylene (HDPE, d=0.4166 and 0.378 nm). The SCS was mounted parallel to the primary beam in a temperature controlled sample holder with mica windows. Static diffraction patterns were collected in 1 minute at 25°C.

2.9 Electron microscopy and ruthenium staining

The SCS was cut into small parts of 1 mm^2 and fixed for one hour with 2% paraformaldehyde and 2.5% glutaraldehyde in a 0.1 m sodium cacodylate buffer at pH 7.4, at room temperature. After rinsing the samples 3 times with PBS, the samples were post-fixated for one hour with 1% osmiumtetroxide in a cacodylate buffer pH 7.4 at 4°C. After rinsing the samples again 3 times with PBS, a second post fixation followed with 0.5% ruthenium tetroxide in distilled water for 30 min at 4°C. Finally, the samples were rinsed again 3 times with PBS, then dehydrated in a 70% ethanol solution and subsequently processed in a series of 70% ethanol:epoxy resin LX112 at a 2:1 ratio v/v for 30 min, 1:1 for 30 min, 1:2 for 30 min and finally 0:1 for 1 h. Then the samples were polymerized for 2 days at 60°C. Subsequently, ultrathin sections of 100 nm thickness were cut with a Reichert Ultracut E microtome (Depew NY, USA) and after staining with 7% uranyl-acetate and a lead citrate solution according to Reynolds (30), the sections were observed and recorded using a Fei Tecnai 12 Twin spirit electron microscope (Hillsboro OR, USA). Of each filter at least 6 images were recorded in order to make an objective observation of the structure inside the lipid membrane.

3. Results

3.1 Influence of the lateral packing on the permeability of excised human SC and the SCS

In order to determine whether the lateral packing affects the permeability of the SC or the SCS, the BA flux is measured as function of temperature between 28 and 46°C. The temperature is increased in steps of 3°C. In figure 2A the flux of BA through SC and SCS is plotted against the temperature. The studies show that the temperature response of the BA diffusion through SC and SCS is remarkably similar over a wide temperature

range; only at the lowest (28°C) and highest (46°C) temperature a significant difference in BA flux is recorded between SCS and SC.

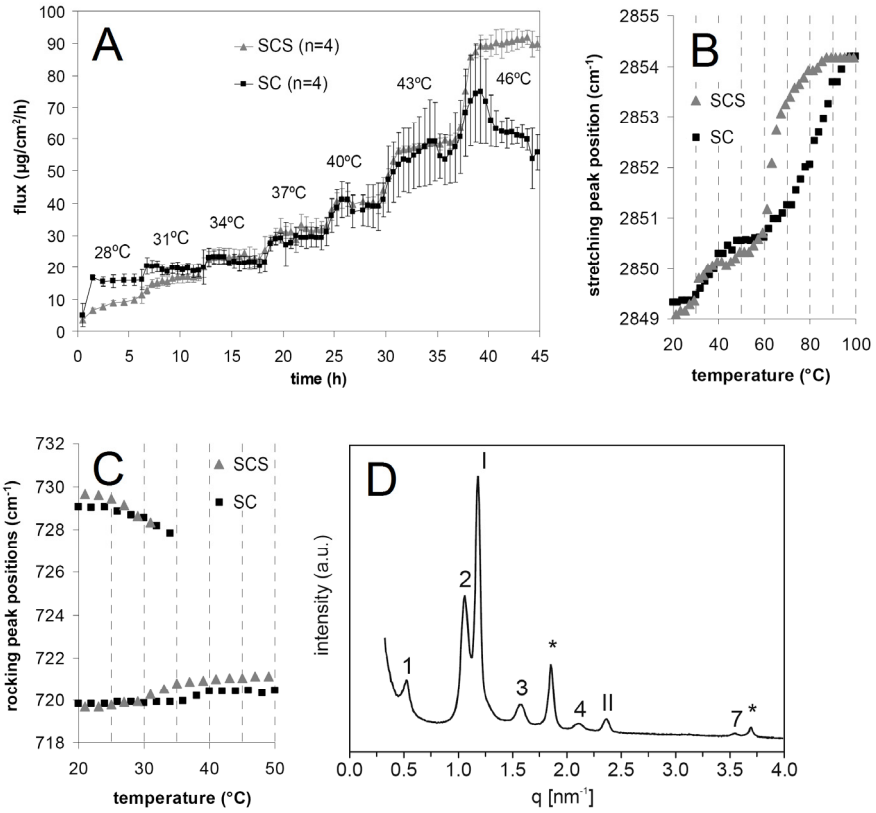

Figure 2: A) The flux of BA through human SC and SCS, at 7 temperature intervals B) FTIR symmetric stretching frequency versus temperature, for SC and SCS C) FTIR rocking frequencies versus temperature, for SC and SCS D) SAXD pattern of SCS. The reflections of the LPP are indicated by Arabic numbers 1-4 and 7, reflections of the SPP are indicated by Roman numbers I and II. Diffraction peaks from crystalline CHOL are indicated by asterisks.

The FTIR CH_2 symmetric stretching frequencies provide information about the conformational ordering of the lipid tails (31, 32). The thermotropic response of the stretching frequencies of SC and SCS is plotted in figure 2B.

At 20°C, for SC and SCS, the stretching frequencies are 2849.3 and 2849.0 cm^{-1} respectively, which indicates a conformational ordering of the CH_2 chains. Upon increasing the temperature, a gradual shift in the stretching frequencies from 2849.4 to 2850.6 is observed between 28°C and 48°C for SC and from 2849.4 to 2850.1 cm^{-1} between 29 and 39°C for SCS, indicating a transition from orthorhombic to hexagonal lateral packing. A further increase in temperature results in a second much stronger shift in frequency from 2850.6 to 2854.2 cm^{-1} between 60 and 97°C for SC and from 2850.5 to 2854.1 cm^{-1} between 55 and 85°C for SCS. This second shift is indicative for the formation of a liquid phase, with midpoint transition temperatures of 81 and 64°C for SC and SCS respectively.

The FTIR rocking frequencies provide detailed information on the lateral packing. Due to short range coupling, the orthorhombic packing is characterized by a doublet at approximately 720 and 730 cm^{-1}, while the hexagonal packing is characterized by a singlet at a vibration frequency of approximately 720 cm^{-1} (33, 34). In figure 2C the rocking frequencies of the FTIR spectrum of SC and SCS are depicted as function of temperature. At 20°C the rocking frequencies are 719.8 and 729.1 cm^{-1} for SC and 719.7 and 729.7 cm^{-1} for SCS, indicating the presence of an orthorhombic packing. Increasing the temperature results in a gradual shift of the high frequency component to 727.8 cm^{-1} at 34°C for SC and to 728.4 cm^{-1} at 31°C for the SCS. A further increase in temperature turns the high frequency component into a shoulder of the low frequency component. This shoulder disappears at around 39°C for SC and 36°C for SCS. The disappearance of the high frequency component marks the endpoint of the orthorhombic to hexagonal transition. A further increase in temperature does not affect the rocking frequencies of SC or SCS.

The SAXD pattern of SCS is shown in figure 2D. It displays two diffraction peaks that can be attributed to the SPP with a periodicity of 5.3 nm and 5 orders of diffraction attributed to the LPP with a periodicity of 12.0

nm. Also, two reflections indicating the presence of crystalline cholesterol are observed.

3.2 Influence of short chain FFA on the barrier function of SCS

In our studies we also focus on the effect of FFA chain length distribution on the lipid organization. This is of interest as e.g. in SC of human reconstructed skin, the fatty acid chain length is reduced compared to that in SC of normal native skin (27). In addition, the presence of shorter FFA may also play a role in the impaired barrier function in diseased skin (35). The SCS prepared with FFA having a shorter chain length is referred to as short FFA SCS.

In figure 3A the flux of BA through SCS and short FFA SCS is plotted. The studies were performed at 3 temperatures: 15, 25 and 33°C. This figure shows that at all three temperatures a significant difference is observed between the steady state flux across SCS and short FFA SCS.

The thermotropic response of the symmetric CH_2 stretching frequencies of the short FFA SCS is depicted in figure 3B. At 20°C, the stretching frequency is around 2849.4 cm^{-1}, indicating a conformational ordering of the lipid tails. Heating results in a gradual increase of the stretching frequencies to 2850.3 at 49°C. A further increase in temperature results in a shift in frequency from 2850.3 to 2852.2 cm^{-1} between 49 and 67°C, indicative for the transition to a liquid phase. The midpoint temperature of this transition is 58°C. Raising the temperature further results in a gradual increase in CH_2 stretching frequency, up to 2853.6 cm^{-1} at 99°C.

As shown in figure 3C, the rocking vibrations in the FTIR spectrum of short FFA SCS display only a single frequency component at 720.8 cm^{-1} between 20 and 50°C, indicating the absence of an orthorhombic lateral packing.

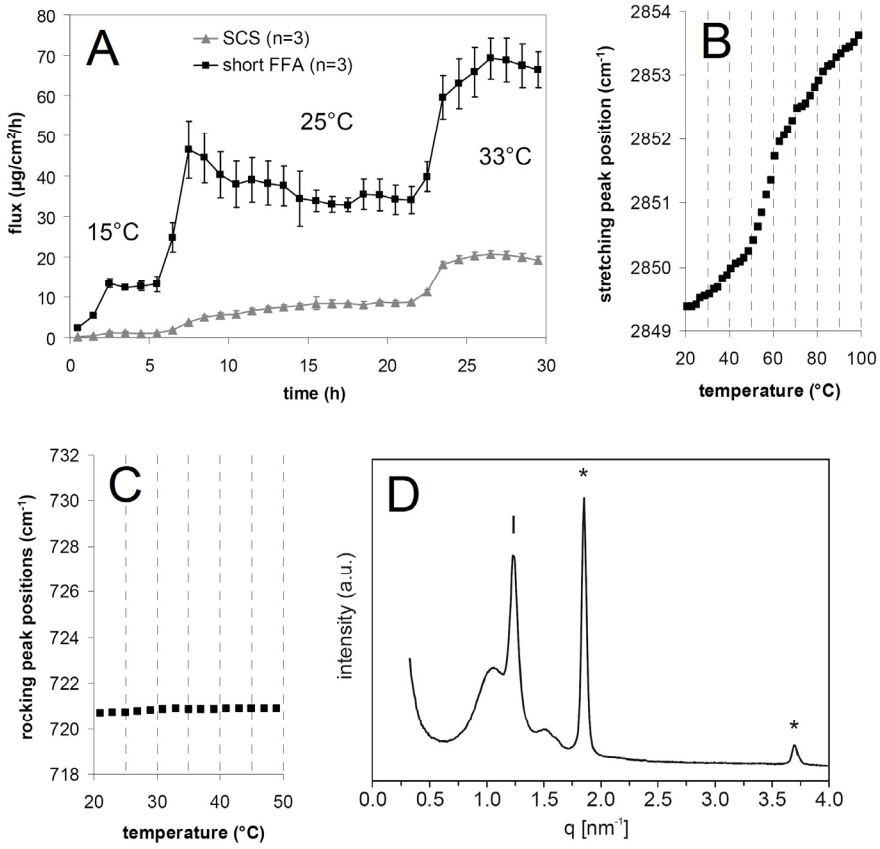

Figure 3: A) The flux of BA through SCS prepared with short chain FFA in comparison with the conventional SCS, at 3 temperature intervals B) FTIR symmetric stretching frequency versus temperature, for the SCS with short chain FFA C) FTIR rocking frequency versus temperature, for the SCS with short chain FFA D) SAXD pattern of the SCS with short chain FFA. One reflection at the position of the first order SPP is indicated by the Roman number I and diffraction peaks from crystalline CHOL are indicated by asterisks.

The SAXD pattern of short FFA SCS displayed in figure 3D shows one sharp diffraction peak at a similar peak position as the 1st order of the

SPP in SCS. Besides this reflection, only very broad peaks are visible around q= 1.0 and 1.5 nm^{-1}. This demonstrates that the long range ordering in the short FFA SCS is very different from that in SCS. Also a relatively large amount of phase-separated crystalline CHOL is present in the short FFA SCS, as can be deducted from the high intensity diffraction peaks at q= 1.85 and 3.7 nm^{-1}.

3.3 Mixing of short chain FFA with CER and CHOL

When using deuterated FFA (denoted as DFFA), due to a shift in the absorption frequencies, the CD_2 and CH_2 scissoring vibrations of the protonated and deuterated FFA respectively, can be monitored simultaneously in the FTIR spectrum. To determine whether the DFFA and CER participate in one lattice or that phase separation occurs, the CD_2 scissoring mode can be monitored. When FFA and CER participate in an orthorhombic packing, the CH_2 and CD_2 scissoring modes will not interact and therefore the vibrational coupling that results in a doublet in the spectrum will be reduced.

In figure 4A the CD_2 scissoring vibrations of the short chain DFFA mixture are depicted. A doublet with positions at 1086 and 1092 cm^{-1} is observed until a temperature of 62°C is reached. This is indicative for the presence of an orthorhombic lateral packing in this temperature range. However, when the CD_2 scissoring mode in the spectrum of the equimolar mixture of CER, CHOL and short chain DFFA is monitored in figure 4B, only a weak doublet of the CD_2 scissoring mode is observed between 20 and 32°C (see arrows). This demonstrates that only a small portion of all DFFA chains has neighboring DFFA chains and that thus the majority of the short chain DFFA and CER molecules participate in the same orthorhombic lattice.

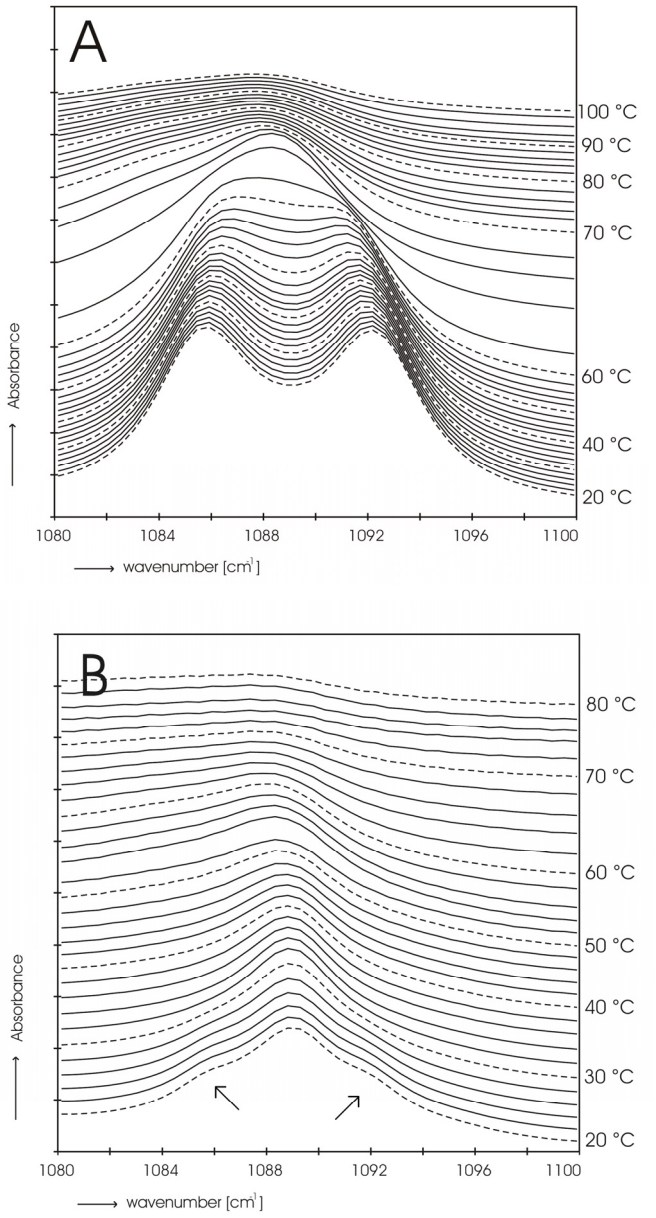

Figure 4: A) Thermotropic CH_2 scissoring spectra of a deuterated short chain FFA mixture depicted from 20 to 100°C. A doublet is observed which disappears at around 62°C. B) Scissoring spectra of DFFA-short in an equimolar mixture with CER and CHOL. Only a weak doublet is observed (indicated by the arrows), which disappears at 32°C.

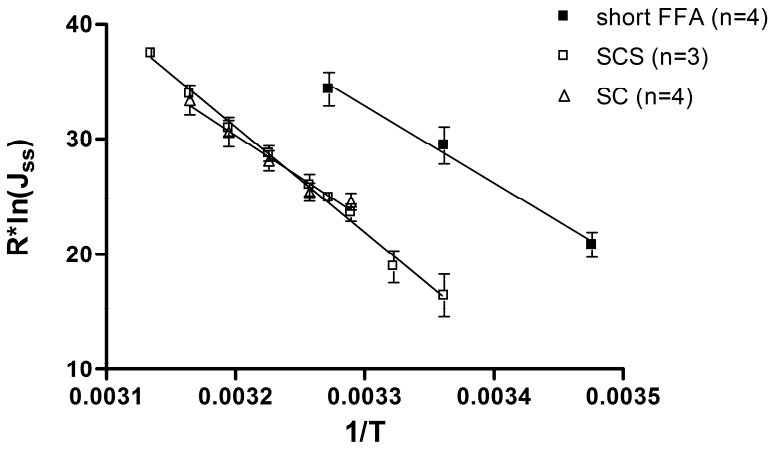

Figure 5: Arrhenius plots for human SC, SCS and short FFA SCS, in which the natural logarithm of the steady state flux (multiplied by the gas constant R), is plotted against the inverse absolute temperature. The linear fit is shown through the flux data of SC and the two models. The error bars in the figure display the standard deviation of the flux data.

3.4 The activation energy for permeation through SC, SCS and the short chain FFA SCS

Figure 5 displays the steady state fluxes obtained at the various temperature intervals for SC, SCS and short FFA SCS, plotted in log scale as function of the reciprocal temperature. Apart from SC at 28 and 46°C and SCS at 15°C (not included because of large flux deviations at these temperatures), for all membranes a linear relationship is observed between the natural logarithm of the steady state flux and the reciprocal temperature. The slope of this linear fit is equal to the activation energy for permeation, see equation 1. Using the same temperature interval for SC and SCS, from 31 to 43°C, the activation energies determined are 73.1 ± 7.1 and 81.9 ± 2.5 kJ/mole for SC and SCS respectively. The appearance of a straight line in figure 5 and thus the existence of only one activation energy in the examined temperature range, indicates that the increase in BA flux as function of

temperature is not affected by the change in packing from an orthorhombic to a hexagonal phase. The activation energy for permeation of BA through the short FFA model is 66.8 ± 5.9 kJ/mole.

3.5 Lamellar structure of SCS and short chain FFA SCS visualised by electron microscopy

In order to obtain further insight into the lamellar organization of the SCS and short FFA SCS, the SCS are visualized in the electron microscope (EM) after embedding and RuO_4 staining. A typical EM image of the SCS is displayed in figure 6A. In this image it is clear that the SCS contains two distinct phases: domains with the well known broad-narrow-broad pattern (36) and darker domains with a repetitive equidistant spacing. In order to establish whether the broad-narrow-broad structure is correlated to the LPP, membranes were prepared with a twofold higher level of CER EOS (as EOS is responsible for the formation of the LPP (37)) and in the absence of CER EOS. When 30% CER EOS was incorporated, the electron microscopic images display predominantly the broad-narrow-broad sequence and very little regions with an equidistant spacing, see figure 6B. When a membrane was prepared in the absence of CER EOS, no broad-narrow-broad structure is visible in the images, see figure 6C. Instead, domains with short periodicity equidistant lamellae are observed, indicating the formation of the SPP. We measured the spacings of the SPP and LPP from figure 6A-C and found that they are somewhat smaller than determined by SAXD, probably due to the embedding process for EM. The lipid organization of the SCS with short chain FFA is displayed in figure 6D. Although lamellae are visible, this image reveals the absence of a well defined stacking of the lipid lamellae and the absence of a broad-narrow-broad pattern.

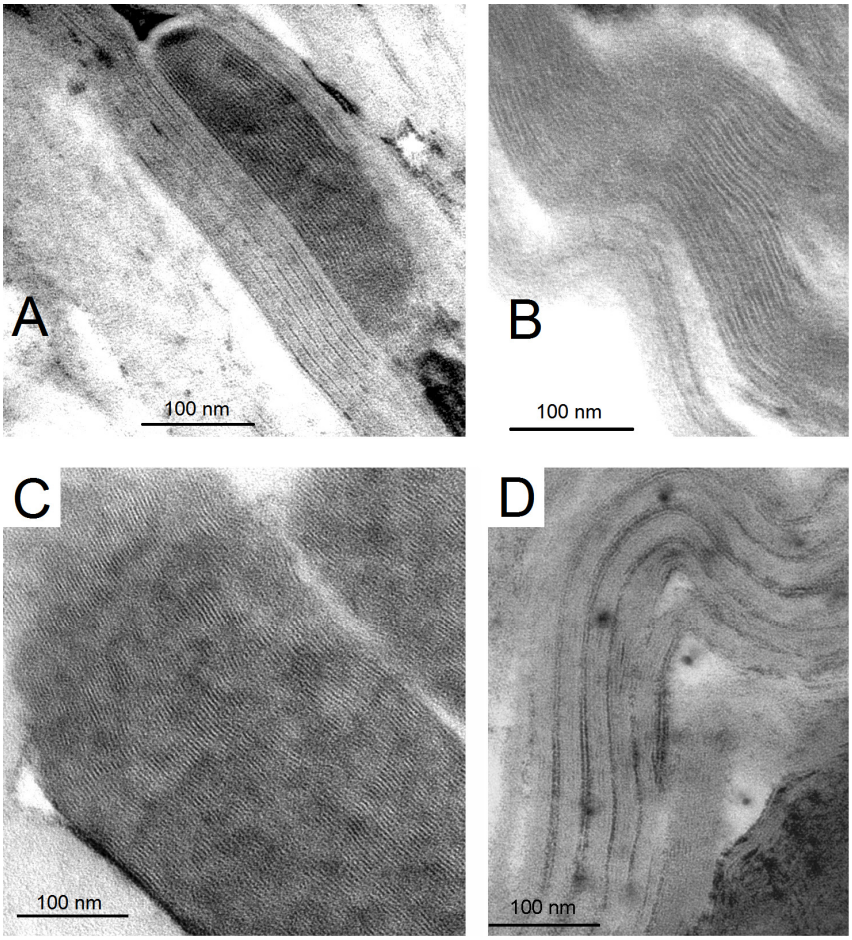

Figure 6: A) Electron microscopy image of the SCS. Two different domains are visible in the micrograph. One domain with the well-known broad-narrow-broad appearance, the other domain with a short repetitive structure. B) EM micrograph of a SCS prepared with a higher level of CER EOS. In this image only lamellae with a broad-narrow-broad pattern are visible. C) Electron microscopy micrograph of a SCS prepared in the absence of CER EOS. In this image only lamellae with a short repetitive pattern are observed. D) EM image of the short FFA SCS. Lamellar structures are visible, but no proper stacking is observed.

4. Discussion

Although it has been suggested that the presence of the orthorhombic phase is important for the skin barrier function, currently there are almost no data available on the effect of the orthorhombic to hexagonal phase transition and the presence of the LPP on the permeability of compounds. Therefore, in this study we examined the effect of the lateral packing on the permeability of SC and SCS by performing diffusion studies in the temperature interval between 15 and 46°C. In addition, the effect of shorter FFA in the SCS on the lipid organization and permeability was examined.

4.1 The permeability of SCS is very similar to human SC

Around the skin temperature (32°C), the steady state fluxes of BA through SC and SCS did not differ significantly. The steady state flux values are around 20 μg/cm^2/h at 32°C, which is very similar to the steady state flux value obtained in a previous study (25). Remarkably, we found that the permeability of SCS to BA closely follows that of human SC at all temperature steps between 31 and 43°C. When comparing SC and SCS in previous studies with PABA, ethyl-PABA and butyl-PABA an excellent correlation between steady state fluxes was also observed (23). Very recently we also noticed that the steady state flux of hydrocortison through SC and SCS is very similar (unpublished results), demonstrating that the SCS mimics the permeation properties of human SC very closely for moderately hydrophilic to moderately lipophilic compounds.

4.2 The activation energy for permeation in SCS and SC is different, but the flux is similar

The E_P values for BA through SC and SCS are consistent with values reported in literature for a range of substances used in skin permeation studies (38). For example, the E_P for acetylsalicylic acid (MW=180, $\log K_{o/w}$=1.19) is 85 kJ/mole (39), for caffeine (MW=194,

$\log K_{o/w}$=0.02) 53 kJ/mole (40), for corticosterone (MW=346, $\log K_{o/w}$=1.94) 97 kJ/mole (41), for ibuprofen (MW=206, $\log K_{o/w}$=3.5) 173 kJ/mole (42) and for water (MW=18, $\log K_{o/w}$=1.38) 57 kJ/mole (2). Mitragotri reports that the E_P for hydrophobic solutes (which also includes BA) is strongly dependent on the molecular size (38). When comparing the E_P calculated for permeation of BA through SC and SCS, the E_P for SC is slightly lower than that for SCS, even though the flux values did not differ significantly between 31 and 43°C. This difference in E_P may be explained by differences in the structure of the SC and SCS: The uniformity in chain length of the synthetic CER in SCS may result in a reduced mismatch between the CER hydrocarbon chains in the lipid lamellae, resulting in a more crystalline structure. Because the environment of the diffusing molecule is affected, this can lead to an increase in E_P (more difficult for the permeant molecule to move through a more crystalline structure).

4.3 Is the orthorhombic lateral packing crucial for a competent SC barrier function?

In previous studies the diffusion of water across pig SC has been measured as function of temperature by Potts and Francoeur (2). From the permeability values an Arrhenius plot can be constructed, which is presented in figure 7. From the linear correlation with the inverse temperature, an E_P of 59.1 ± 2.9 kJ/mole can be calculated. Porcine SC does not exhibit an orthorhombic-hexagonal phase transition (43), demonstrating that in the absence of a phase transition a linear correlation is observed between the log of the steady state flux and the inverse absolute temperature. In human SC and the SCS, the rocking frequencies as function of temperature demonstrated that an orthorhombic to hexagonal phase transition occurs between 30 and 40°C. However, when focusing on the Arrhenius plot of human SC and SCS, a linear relationship is observed similar to that in pig SC. This demonstrates that the orthorhombic-hexagonal phase transition

does not affect E_p and therefore does not affect the diffusivity of BA across human SC and the SCS (29).

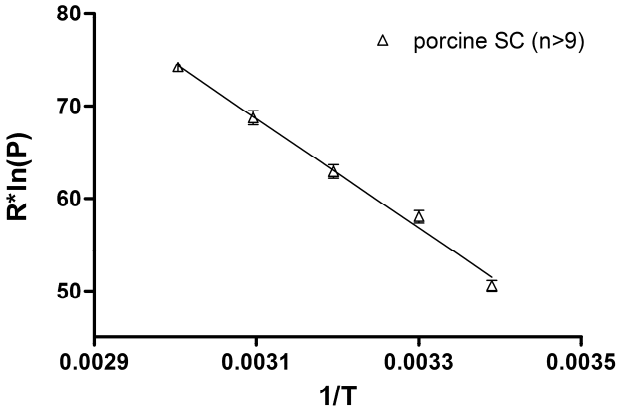

Figure 7: Arrhenius plot for water permeation through porcine SC. The permeation data were presented in an earlier study by Potts and Francoeur (2). Shown in the plot is the linear fit through the flux data. Error bars in the figure represent the standard error of the mean.

Although our studies have only been carried out with BA and the diffusion of other compounds may be more sensitive to the orthorhombic-hexagonal phase transition, our results demonstrate that the presence of the orthorhombic lateral packing seems to be less crucial than suggested in previous studies (21, 26, 44, 45).

In SC of human skin equivalents the lipids form the LPP very similar to that in native SC, but the lateral packing of the lipids is hexagonal (27), very similar to that in porcine SC. Permeation studies have shown that the methyl nicotinate flux across human skin equivalents is 2-fold higher than observed for native human skin (46). However, the results of our present study indicate that the hexagonal lateral packing may not explain this increased permeability.

The results discussed above are in contrast with those of a recent study focusing on the permeation of water through human SC (26). In this study it is reported that the water transport is influenced by the relative population of lipids forming an orthorhombic packing. However, in the latter study the TEWL has been used as a measure for the water transport. Perhaps the difference in physical properties of the solute (water versus BA) or the difference between inside-out permeation (TEWL) and outside-in permeation (BA permeation) can account for the different observations. In a study of Chilcott et al (47), it was shown that TEWL and diffusion of substances, both measured in vitro, do not correlate.

4.4 The formation of ordered lamellar phases is crucial for the SC barrier function

The BA flux through the SCS prepared with short chain FFA is approximately 4-fold higher than that through normal SCS. This was observed at all three temperatures selected in the studies. In addition the E_p is lower than that of normal SCS. When comparing the short FFA SCS with the SCS, differences in lipid organization are noticed. As far as the lateral packing is concerned, at skin temperature a hexagonal lateral packing is observed. However, as discussed above, for BA no obvious difference in diffusivity is expected between a hexagonal and an orthorhombic lateral packing. Therefore, the absence of the orthorhombic packing cannot explain the high permeability observed in the short FFA SCS, provided that the penetration pathlength remains the same in both the hexagonal and ortorhombic lateral packing (see equation 2). As in this model the chain length difference between the short chain FFA and the CER is substantial, phase separation within the crystalline lattice is likely to occur and was therefore examined using SCS prepared with DFFA. These studies, however, demonstrated that the short chain FFA and the CER both participate in the same lattice. Phase separation can therefore not contribute to the increase in BA flux. When focusing on the lamellar organization, the

lipids in the short chain FFA SCS form different phases than observed in the SCS: in the X-ray diffraction pattern no LPP is noticed and only one reflection can be attributed to the SPP. Instead, broad reflections are observed that are absent in the diffraction pattern of the normal SCS, indicating the absence of a proper stacking of the lipid lamellae. This is confirmed by the electron microscopic studies of the short FFA SCS. In a previous study it was shown that a lack of the LPP results in a 2-fold increased flux of ethyl-para amino benzoic acid (23). Because no LPP is formed and the stacking of the lamellae is less defined, the pathlength through the short FFA membrane may be significantly reduced. The diffusivity of the short FFA membrane (calculated from E_P with equation 1) is only slightly different from the diffusivity of the SCS. Therefore, the absence of the proper lamellar phases may account for the increased flux through the short FFA SCS by reducing the pathlength for permeation (see equation 2).

Interestingly, with EM in the SCS two domains with a different appearance could be distinguished; the broad-narrow-broad pattern and the short repetitive pattern. Although the LPP has been related to the broad-narrow-broad pattern in previous studies (36), until now, this relation was not completely established. For this reason, we prepared a SCS in the absence of the CER EOS and a SCS with 30% CER EOS. X-ray diffraction studies showed that in the absence of CER EOS only the SPP is formed (37), while with 30% CER EOS in our mixture the LPP is predominantly formed (unpublished results). These findings correlate excellently with the presence of mainly broad-narrow-broad pattern in the EM images of the SCS with 30% CER EOS and the presence of only the short repetition pattern in SCS prepared without EOS. Therefore these studies demonstrate that the broad-narrow-broad pattern is indeed directly related to the LPP.

When extrapolating our findings to SC of diseased skin, our present studies suggest that the skin barrier function is more sensitive to a change in the lamellar phases than to a change from an orthorhombic to a hexagonal lateral packing. In lamellar Ichthyosis (48, 49) as well as in psoriasis SC

(unpublished results) the lamellar phases are different from that in SC of healthy human subjects.

In conclusion, we observed that the permeability of BA through human SC and the SCS is not affected by the orthorhombic-hexagonal transition. However, when substituting the long chain FFA for short chain FFA an increased permeability was observed due to a drastic change in the lamellar organization. Our studies indicate that the absence of a proper lamellar organization has a higher impact on the skin barrier function than a change from orthorhombic to hexagonal lateral packing. These findings may provide new insights into the skin barrier function, especially in diseased skin.

Acknowledgments

This work was supported by a grant from the Technology Foundation STW (LGP 7503). We thank the company Cosmoferm B.V. (Evonik) for the provision of the ceramides and the Netherlands Organization for Scientific Research (NWO) for the provision of beam time at the ESRF. Furthermore we thank the personnel at the DUBBLE beam line at the ESRF for their support with the x-ray measurements. Finally, we thank Aat Mulder for the EM studies, Drs Michelle Janssens for additional FTIR measurements and Dr Maria Ponec for valuable discussions about the permeability studies.

References

1. Motta, S., M. Monti, S. Sesana, R. Caputo, S. Carelli, and R. Ghidoni. 1993. Ceramide composition of the psoriatic scale. Biochim. Biophys. Acta 1182:147-151.
2. Potts, R. O., and M. L. Francoeur. 1990. Lipid biophysics of water loss through the skin. Proc Natl Acad Sci U S A 87:3871-3873.
3. Simonetti, O., A. J. Hoogstraate, W. Bialik, J. A. Kempenaar, A. H. Schrijvers, H. E. Bodde, and M. Ponec. 1995. Visualization of diffusion pathways across the stratum corneum of native and in-vitro-reconstructed epidermis by confocal laser scanning microscopy. Arch Dermatol Res 287:465-473.
4. Wertz, P. W., M. C. Miethke, S. A. Long, J. S. Strauss, and D. T. Downing. 1985. The composition of the ceramides from human stratum corneum and from comedones. J. Invest. Dermatol. 84:410-412.
5. Robson, K. J., M. E. Stewart, S. Michelsen, N. D. Lazo, and D. T. Downing. 1994. 6-Hydroxy-4-sphingenine in human epidermal ceramides. J. Lipid. Res. 35:2060-2068.
6. Stewart, M. E., and D. T. Downing. 1999. A new 6-hydroxy-4-sphingenine-containing ceramide in human skin. J. Lipid. Res. 40:1434-1439.
7. Ponec, M., A. Weerheim, P. Lankhorst, and P. Wertz. 2003. New acylceramide in native and reconstructed epidermis. J. Invest. Dermatol. 120:581-588.
8. Masukawa, Y., H. Narita, E. Shimizu, N. Kondo, Y. Sugai, T. Oba, R. Homma, J. Ishikawa, Y. Takagi, T. Kitahara, Y. Takema, and K. Kita. 2008. Characterization of overall ceramide species in human stratum corneum. J Lipid Res 49:1466-1476.
9. Bouwstra, J. A., G. S. Gooris, J. A. van der Spek, and W. Bras. 1991. Structural investigations of human stratum corneum by small-angle X-ray scattering. J. Invest. Dermatol. 97:1005-1012.
10. Bouwstra, J. A., G. S. Gooris, W. Bras, and D. T. Downing. 1995. Lipid organization in pig stratum corneum. J. Lipid Res. 36:685-695.
11. White, S. H., D. Mirejovsky, and G. I. King. 1988. Structure of lamellar lipid domains and corneocyte envelopes of murine stratum corneum. An X-ray diffraction study. Biochemistry 27:3725-3732.
12. Bouwstra, J., G. Gooris, and M. Ponec. 2002. The lipid organisation of the skin barrier: liquid and crystalline domains coexist in lamellar phases. journal of Biological Physics 28:211-223.
13. Hatta, I., N. Ohta, K. Inoue, and N. Yagi. 2006. Coexistence of two domains in intercellular lipid matrix of stratum corneum. Biochim Biophys Acta 1758:1830-1836.

14. Wertz, P. 1991. Epidermal lipids. In Physiology, Biochemistry and Molecular Biology of the Skin. L. A. Goldsmith, editor. Oxford University Press, Oxford. 205-235.
15. Swartzendruber, D. C., P. W. Wertz, D. J. Kitko, K. C. Madison, and D. T. Downing. 1989. Molecular models of the intercellular lipid lamellae in mammalian stratum corneum. J Invest Dermatol 92:251-257.
16. Bouwstra, J. A., G. S. Gooris, K. Cheng, A. Weerheim, W. Bras, and M. Ponec. 1996. Phase behavior of isolated skin lipids. J. Lipid Res. 37:999-1011.
17. Bouwstra, J. A., G. S. Gooris, F. E. Dubbelaar, A. M. Weerheim, and M. Ponec. 1998. pH, cholesterol sulfate, and fatty acids affect the stratum corneum lipid organization. J Investig Dermatol Symp Proc 3:69-74.
18. Moore, D. J., and M. E. Rerek. 2000. Insights into the molecular organization of lipids in the skin barrier from infrared spectroscopy studies of stratum corneum lipid models. Acta Derm Venereol Suppl (Stockh) 208:16-22.
19. McIntosh, T. J. 2003. Organization of skin stratum corneum extracellular lamellae: diffraction evidence for asymmetric distribution of cholesterol. Biophys J 85:1675-1681.
20. Kiselev, M. A., N. Y. Ryabova, A. M. Balagurov, S. Dante, T. Hauss, J. Zbytovska, S. Wartewig, and R. H. Neubert. 2005. New insights into the structure and hydration of a stratum corneum lipid model membrane by neutron diffraction. Eur Biophys J 34:1030-1040.
21. Bouwstra, J. A., and M. Ponec. 2006. The skin barrier in healthy and diseased state. Biochim Biophys Acta 1758:2080-2095.
22. Kessner, D., A. Ruettinger, M. A. Kiselev, S. Wartewig, and R. H. Neubert. 2008. Properties of ceramides and their impact on the stratum corneum structure. Part 2: stratum corneum lipid model systems. Skin Pharmacol Physiol 21:58-74.
23. de Jager, M., W. Groenink, R. Bielsa i Guivernau, E. Andersson, N. Angelova, M. Ponec, and J. Bouwstra. 2006. A novel in vitro percutaneous penetration model: evaluation of barrier properties with p-aminobenzoic acid and two of its derivatives. Pharm. Res. 23:951-960.
24. de Jager, M., W. Groenink, J. van der Spek, C. Janmaat, G. Gooris, M. Ponec, and J. Bouwstra. 2006. Preparation and characterization of a stratum corneum substitute for in vitro percutaneous penetration studies. Biochim. Biophys. Acta 1758:636-644.
25. Groen, D., G. S. Gooris, M. Ponec, and J. A. Bouwstra. 2008. Two new methods for preparing a unique stratum corneum substitute. Biochim Biophys Acta 1778:2421-2429.
26. Damien, F., and M. Boncheva. 2010. The extent of orthorhombic lipid phases in the stratum corneum determines the barrier efficiency of human skin in vivo. J Invest Dermatol 130:611-614.

27. Ponec, M., S. Gibbs, G. Pilgram, E. Boelsma, H. Koerten, J. Bouwstra, and M. Mommaas. 2001. Barrier function in reconstructed epidermis and its resemblance to native human skin. Skin Pharmacol Appl Skin Physiol 14 Suppl 1:63-71.
28. Gooris, G. S., and J. A. Bouwstra. 2007. Infrared spectroscopic study of stratum corneum model membranes prepared from human ceramides, cholesterol, and fatty acids. Biophys J 92:2785-2795.
29. Barry, B. W. 1983. Dermatological Formulations: Percutaneous Absorption. Marcel Dekker, inc, New York.
30. Reynolds, E. S. 1963. The use of lead citrate at high pH as an electron-opaque stain in electron microscopy. J Cell Biol 17:208-212.
31. Snyder, R. G., S. L. Hsu, and S. Krimm. 1978. Vibrational-Spectra in C-H Stretching Region and Structure of Polymethylene Chain. Spectrochimica Acta Part a-Molecular and Biomolecular Spectroscopy 34:395-406.
32. Wolfangel, P., R. Lehnert, H. H. Meyer, and K. Muller. 1999. FTIR studies of phospholipid membranes containing monoacetylenic acyl chains. Physical Chemistry Chemical Physics 1:4833-4841.
33. Snyder, R. G. 1960. Vibrational Spectra of Crystalline N-Paraffins .1. Methylene Rocking and Wagging Modes. Journal of Molecular Spectroscopy 4:411-434.
34. Moore, D. J., M. E. Rerek, and R. Mendelsohn. 1997. Lipid domains and orthorhombic phases in model stratum corneum: Evidence from Fourier transform infrared spectroscopy studies. Biochemical and Biophysical Research Communications 231:797-801.
35. Ishikawa, J., H. Narita, N. Kondo, M. Hotta, Y. Takagi, Y. Masukawa, T. Kitahara, Y. Takema, S. Koyano, S. Yamazaki, and A. Hatamochi. Changes in the Ceramide Profile of Atopic Dermatitis Patients. J Invest Dermatol.
36. Madison, K. C., D. C. Swartzendruber, P. W. Wertz, and D. T. Downing. 1987. Presence of intact intercellular lipid lamellae in the upper layers of the stratum corneum. J Invest Dermatol 88:714-718.
37. Bouwstra, J. A., G. S. Gooris, F. E. Dubbelaar, A. M. Weerheim, A. P. Ijzerman, and M. Ponec. 1998. Role of ceramide 1 in the molecular organization of the stratum corneum lipids. J Lipid Res 39:186-196.
38. Mitragotri, S. 2007. Temperature dependence of skin permeability to hydrophilic and hydrophobic solutes. J Pharm Sci 96:1832-1839.
39. Scheuplein, R. J., and I. H. Blank. 1971. Permeability of the skin. Physiol Rev 51:702-747.
40. Akomeah, F., T. Nazir, G. P. Martin, and M. B. Brown. 2004. Effect of heat on the percutaneous absorption and skin retention of three model penetrants. Eur J Pharm Sci 21:337-345.

41. Peck, K. D., A. H. Ghanem, and W. I. Higuchi. 1995. The effect of temperature upon the permeation of polar and ionic solutes through human epidermal membrane. J Pharm Sci 84:975-982.
42. Ito, Y., T. Ogiso, and M. Iwaki. 1988. Thermodynamic study on enhancement of percutaneous penetration of drugs by Azone. J Pharmacobiodyn 11:749-757.
43. Caussin, J., G. S. Gooris, M. Janssens, and J. A. Bouwstra. 2008. Lipid organization in human and porcine stratum corneum differs widely, while lipid mixtures with porcine ceramides model human stratum corneum lipid organization very closely. Biochim Biophys Acta 1778:1472-1482.
44. Bommannan, D., R. O. Potts, and R. H. Guy. 1990. Examination of stratum corneum barrier function in vivo by infrared spectroscopy. J Invest Dermatol 95:403-408.
45. Moore, D. J., R. G. Snyder, M. E. Rerek, and R. Mendelsohn. 2006. Kinetics of membrane raft formation: fatty acid domains in stratum corneum lipid models. J Phys Chem B 110:2378-2386.
46. Boelsma, E., C. Anderson, A. M. Karlsson, and M. Ponec. 2000. Microdialysis technique as a method to study the percutaneous penetration of methyl nicotinate through excised human skin, reconstructed epidermis, and human skin in vivo. Pharm Res 17:141-147.
47. Chilcott, R. P., C. H. Dalton, A. J. Emmanuel, C. E. Allen, and S. T. Bradley. 2002. Transepidermal water loss does not correlate with skin barrier function in vitro. J Invest Dermatol 118:871-875.
48. Lavrijsen, A. P., J. A. Bouwstra, G. S. Gooris, A. Weerheim, H. E. Bodde, and M. Ponec. 1995. Reduced skin barrier function parallels abnormal stratum corneum lipid organization in patients with lamellar ichthyosis. J Invest Dermatol 105:619-624.
49. Pilgram, G. S., D. C. Vissers, H. van der Meulen, S. Pavel, S. P. Lavrijsen, J. A. Bouwstra, and H. K. Koerten. 2001. Aberrant lipid organization in stratum corneum of patients with atopic dermatitis and lamellar ichthyosis. J Invest Dermatol 117:710-717.